World Applied Sciences Journal 24 (10): 1390-1398, 2013
ISSN 1818-4952

DOI: 10.5829/idosi.wasj.2013.24.10.1307

Chemical Reaction and Uniform Heat Generation or Absorption Effects on MHD Stagnation-Point Flow of a Nanofluid over a Porous Sheet

[1,2]Imran Anwar, [1]Abdul Rahman Mohd Kasim, [1]Zulkibri Ismail, [3]Mohd Zuki Salleh and [1]Sharidan Shafie

[1]Department of Mathematical Sciences, Faculty of Science,
Universiti Teknologi Malaysia 81310 UTM Skudai, JOHOR, Malaysia
[2]Department of Mathematics, Faculty of Science, University of Sargodha, Pakistan
[3]Faculty of Industrial Science and Technology,
Universiti Malaysia Pahang 26300 UMP Kuantan, Pahang, Malaysia

Submitted: Aug 2, 2013; **Accepted:** Sep 10, 2013; **Published:** Sep 15, 2013

Abstract: The objective of this work is to analyze the chemical reaction and heat generation or absorption effects on MHD stagnation-point flow of a nanofluid over a porous stretching sheet. The uniform magnetic field strength B is applied in the direction normal to the flow. A highly nonlinear problem of nanofluid is modeled for the modified Bernoulli's equation of an electrically conducting nanofluid by incorporating the effects of embedded flow parameters such as Brownian motion parameter, thermophoresis parameter, velocity ratio parameter, heat generation/absorption parameter, suction or injection parameter, chemical reaction parameter, Hartmann number, Prandtl number and Lewis number. A system of nonlinear partial differential equations is reduced to nonlinear ordinary differential equations and then solved using finite difference scheme known as the Keller-box method. A parametric study of the involved physical parameters is conducted and a set of numerical results is illustrated in graphical and tabular forms. A comparison with published results is also provided.

Key words: Chemical reaction % Nanofluid % MHD flow % Stagnation-point % Porous stretching sheet

INTRODUCTION

During the past decades, study of boundary layer flow of nanofluid is a hot area for several investigations and a literature on nanofluid is continuously growing up. Currently, researchers are taking keen interest in their studies not only that nanofluid is less explored compare to other fluids but also due to vital role of nanofluid in industrial and medical fields and their various practical applications [1,2]. Few of these applications are found in magnetic cell separation, drug delivery, hyperthermia and constant enhancement in magnetic resonance imaging [3]. Further, the thermal conductivity of nanofluid has a significant impact on the heat transfer coefficient between the heat transfer medium and heat transfer surface [4]. Putra *et al*. [5] were the first to study natural convection flow of nanofluid by using water as a base fluid. They showed that the natural convective heat transfer is lower in nanofluid than in pure water. This decrease in natural convection heat transfer coefficient increases with particle concentration. Kuznetsov and Nield [6] presented similarity solutions to study natural convective boundary layer flow of a nanofluid past a vertical plate. Moreover, these flows induced by a stretching surface are of much importance in manufacturing processes of artificial films and wires, glass manufacturing and paper production [7].

In fluid mechanics problems, the point in the flow field where local velocity of the fluid becomes zero is called a stagnation-point. This point exists at the surface of the object where the fluid is brought to be at rest because of a force exerted by the object. Bernoulli equation shows that the total pressure in terms of static pressure called stagnation pressure is at maximum value when the fluid velocity is zero [8]. In conjunction with

Corresponding Author: Sharidan Shafie, Department of Mathematical Sciences, Faculty of Science,
Universiti Teknologi Malaysia 81310 UTM Skudai, Johor, Malaysia. E-mail: ridafie@yahoo.com.

heat and mass transfer, a primary interest on stagnation-point flow towards a stretching sheet has drawn a considerable attention for several researchers. The conjugate effects of heat and mass transfer play an important role in designing of chemical processing equipment, chemical reactor process engineering, geochemical systems, formation and dispersion of fog, distribution of temperature and moisture over agricultural fields and groves of fruit trees and crop damage due to freezing and environmental pollution [9-11]. Mustafa *et al*. [12] investigated the steady two dimensional stagnation-point flow of a nanofluid towards a stretching sheet.

In most of the chemical engineering processes, there is a chemical reaction between a foreign mass and the fluid. These processes take place in numerous industrial applications such as manufacturing of ceramics, food processing and polymer production [13]. Muthucumaraswamy [14] studied the effects of chemical reaction on vertical oscillating plate with variable temperature whereas Muthucumaraswamy and Manivannan [15] investigated first order chemical reaction on isothermal vertical oscillating plate with variable mass diffusion. Chamkha and Issa [16] investigated chemical reaction, heat generation or absorption effects on MHD boundary layer flow over a permeable stretching surface. However, such studies for nanofluid are rarely available in the literature especially when conjugate effects of heat and mass transfer are considered [17].

Alsaedi *et al*. [18] analyzed the stagnation-point flow of nanofluid near a permeable stretching surface. In additions, MHD flows have applications in MHD power generators, MHD pumps, flow meters and accelerators, plasma studies, nuclear reactor using liquid metal coolant and geothermal energy extraction as well as in flight magnetohydrodynamics [19-21]. Ouaf [22] studied the effect of thermal radiation on MHD axi-symmetric flow of an electrically conducting fluid past a permeable stretching sheet. Hamad and Ferdows [23] studied a stagnation-point flow of a nanofluid over a permeable stretching sheet in porous medium with heat generation or absorption effects.

Having in mind the above motivation, the present work of nanofluid concentrates on the simultaneous heat and mass transfer in the presence of chemical reaction, heat generation or absorption when the MHD stagnation-point flow of a nanofluid is considered over a porous (permeable) stretching sheet. This area of research has important applications in nuclear reactor cooling systems, biomedicine, electronics, glass fiber, hot rolling, food and transportation [24, 25]. To the best of author's knowledge, such studies are not reported in the literature and all the included results are new.

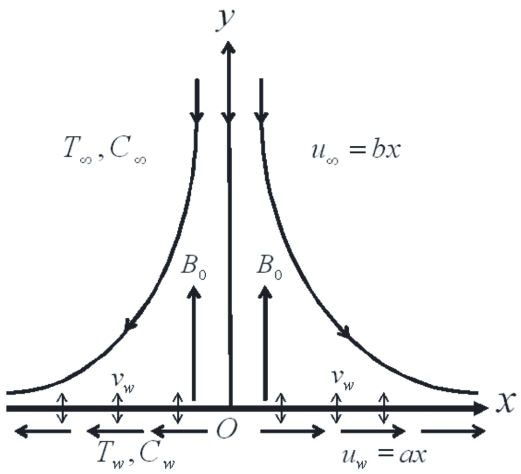

Fig. 1: Physical model and coordinate system.

Problem Formulation: A steady two-dimensional boundary layer stagnation-point flow of a nanofluid past a permeable stretching sheet in the presence of a chemical reaction is considered, where fluid motions are influenced by heat generation or absorption effects. The stretching and free stream velocities are assumed to be of the forms $u_w(x) = ax$ and $u_\infty(x) = bx$ respectively, where *a*, *b* are constant parameters and *x* is the coordinate measured along the stretching surface. A uniform transverse magnetic field of strength B is imposed in the *y*- direction normal to the flat sheet. It is assumed that the induced magnetic field due to the motion of an electrically conducting fluid is negligible. Further, it is also assumed that the external electrical field is zero and the electric field due to the polarization of charges is negligible [11]. The temperature *T* and the nanoparticles fraction *C* take constant values T_w and C_w respectively, whereas the ambient values of temperature T_4 and the nanoparticles fraction C_4 are attained as *y* tends to infinity as shown in Fig. 1.

By neglecting viscous dissipation, the boundary layer equations governing the flow are given as follows

$$\frac{\partial u}{\partial x} + \frac{\partial v}{\partial y} = 0, \tag{1}$$

$$u\frac{\partial u}{\partial x} + v\frac{\partial u}{\partial y} = u_\infty \frac{du_\infty}{dx} + \frac{m}{r_f}\frac{\partial^2 u}{\partial y^2} + \frac{s\,B_0^2}{r_f}\left(u_\infty - u\right), \tag{2}$$

$$u\frac{\partial T}{\partial x}+v\frac{\partial T}{\partial y}=\frac{k}{(rc)_f}\frac{\partial^2 T}{\partial y^2}+\frac{Q_0}{r_f c_p}(T-T_\infty)+\frac{(rc)_p}{(rc)_f}\left[D_B\frac{\partial C}{\partial y}\frac{\partial T}{\partial y}+\frac{D_T}{T_\infty}\left(\frac{\partial T}{\partial y}\right)^2\right], \quad (3)$$

$$u\frac{\partial C}{\partial x}+v\frac{\partial C}{\partial y}=D_B\frac{\partial^2 C}{\partial y^2}+\frac{D_T}{T_\infty}\frac{\partial^2 T}{\partial y^2}-R_0(C-C_\infty), \quad (4)$$

where u and v are the velocity components in the x and y-directions respectively, μ is the viscosity, ρ_f is the density of the base fluid, σ is the electrical conductivity, B_0 is the uniform magnetic field strength, $(\rho c)_f$ is the heat capacitance of the base fluid, Q_0 is the heat generation or absorption coefficient, c_p is the specific heat, $(\rho c)_p$ is the heat capacitance of the nanoparticles, D_B is the Brownian diffusion coefficient, D_T is the thermophoresis diffusion coefficient and R_0 is the chemical reaction coefficient. The associated boundary conditions are

$$\begin{aligned} &u=u_w(x)=ax,\ v=v_w,\\ &T=T_w,\ C=C_w \ \text{ at } \ y=0,\\ &u\to u_\infty(x)=bx,\ v\to 0,\\ &T\to T_\infty,\ C\to C_\infty \text{ as } y\to\infty, \end{aligned} \quad (5)$$

By introducing a stream function $\psi = \psi(x,y)$ the continuity Eq. (1) is satisfied identically for

$$u=\frac{\partial y}{\partial y},\ v=-\frac{\partial y}{\partial x}. \quad (6)$$

Following Khan and Pop [26], similarity transformation is defined as follows

$$\begin{aligned} &u=axf'(h),\ v=-\sqrt{an}\,f(h),\ h=y\sqrt{a/n},\\ &q(h)=\frac{T-T_\infty}{T_w-T_\infty},\ f(h)=\frac{C-C_\infty}{C_w-C_\infty}. \end{aligned} \quad (7)$$

On substituting Eq. (7) into Eqs. (1), (2), (3) and (4), we get the coupled system of ordinary differential equations,

$$f'''+ff''-f'^2+e^2-M(f'-e)=0, \quad (8)$$

$$\frac{1}{\Pr}q''+fq'+lq+Nbf'q'+Ntq'^2=0, \quad (9)$$

$$f''+Lef f'+\frac{Nt}{Nb}q''-LeRf=0, \quad (10)$$

where

$$\begin{aligned} &e=\frac{b}{a},\ n=\frac{m}{r_f},\ M=\frac{s B_0^2}{a r_f},\ \Pr=\frac{n(rc)_f}{k},\\ &l=\frac{Q_0}{a r_f c_p},\ Le=\frac{n}{D_B},\ Nb=\frac{(rc)_p D_B}{n(rc)_f}(C_w-C_\infty),\\ &Nt=\frac{(rc)_p D_T}{(rc)_f n T_\infty}(T_w-T_\infty),\ R=\frac{R_0}{a},\ S=\frac{v_w}{\sqrt{an}}. \end{aligned} \quad (11)$$

Here γ is the velocity ratio parameter, ν is the kinematic viscosity of the fluid, M is the magnetic parameter called Hartmann number, Pr is the Prandtl number, δ is the heat source ($\delta > 0$) or sink parameter ($\delta < 0$), Le is the Lewis number, Nb is the Brownian motion parameter, Nt is the thermophoresis parameter, R is the is the chemical reaction parameter and S is the suction ($S > 0$) or injection or blowing parameter ($S < 0$). The corresponding boundary conditions are transformed into

$$\begin{aligned} &f(h)=S,\ f'(h)=1,\ q(h)=1,\ f(h)=1 \ \text{ at } \ h=0,\\ &f'(h)\to e,\ q(h)\to 0,\ f(h)\to 0 \ \text{ as } \ h\to\infty, \end{aligned} \quad (12)$$

where $S=\frac{-v_w}{\sqrt{an}}$ is the suction ($S > 0$) or injection ($S < 0$) parameter. The special interests and significance of the present problem of nanofluid for the conjugate effects of heat and mass transfer are the Nusselt number, Sherwood number and skin-friction defined as

$$Nu_x=\frac{xq_w}{k(T_w-T_\infty)},\ Sh_x=\frac{xq_m}{D_B(C_w-C_\infty)},\ C_f=\frac{t_w}{r_f u_w^2}, \quad (13)$$

where

$$q_w=-k\frac{\partial T}{\partial y},\ q_m=-D_B\frac{\partial C}{\partial y},\ t_w=m\frac{\partial u}{\partial y}, \quad \text{at } y=0. \quad (14)$$

The associated expressions of dimensionless reduced Nusselt number $-q'(0)$, reduced Sherwood number $-f'(0)$ and skin-friction coefficient $C_{fx}(0)=f''(0)$ are defined as [15]

$$-q'(0)=\frac{Nu}{\sqrt{\mathrm{Re}_x}},\ -f'(0)=\frac{Sh}{\sqrt{\mathrm{Re}_x}},\ C_{fx}(0)=C_f\sqrt{\mathrm{Re}_x}. \quad (15)$$

Where $\mathrm{Re}_x = u_w(x)/\nu$ is the local Reynolds number based on the permeable stretching sheet. The transformed system of nonlinear ordinary differential Eqs. (8)-(10) subjected to the boundary conditions (12) is solved numerically by means of Keller-box method [26].

RESULTS AND DISCUSSION

This section deals with the numerical solutions of the transformed nonlinear ordinary differential Eqs. (8)-(10) subjected to the boundary conditions (12) by using finite difference scheme known as the Keller-box method [26]. Results for physical parameters of interest such as Brownian motion parameter *Nb*, thermophoresis parameter *Nt*, chemical reaction parameter *R*, heat generation or absorption parameter δ, suction or injection parameter *S*, velocity ratio parameter γ, Hartmann number *M*, Prandtl number Pr and Lewis number *Le* are shown in Tables 1, 2 and displayed graphically through Figs. 2 to 14. Table 1 shows the comparison of the present results (when *M*, *S*, *R*, δ and γ are equal to zero) for the reduced Nusselt number $-q'(0)$ and the reduced Sherwood number $-f'(0)$ with the results obtained by Khan and Pop [28] and found in a good agreement.

Table 2 is prepared for different values of *Nb*, *Nt*, Pr, *Le*, *M*, *R*, *S* and δ to show the variations of $-q'(0)$, $-f'(0)$ and $C_{fx}(0)$. It is observed that $-f'(0)$ increases for the increasing values of Pr, γ, $S > 0$, $\delta < 0$ and decreases for the increasing values of *Nb*, *Nt*, *Le*, *R*, $S < 0$ and $\delta > 0$. On the other hand, it is found that $-f'(0)$ decreases for the increasing values of $S < 0$, $\delta < 0$ whereas increases for the increasing values of *Nb*, *Nt*, Pr, *Le*, *R*, $S > 0$, $\delta > 0$ and γ. Also, it is noted that $-q'(0)$ and $-f'(0)$ decreases for the increasing values of *M* when $\gamma < 1$ whereas increases for the case when $\gamma < 1$. Moreover, it is observed that $C_{fx}(0)$ decreases for the increasing values of γ and $S < 0$ whereas increases for the increasing values of *M* and $S > 0$ when $\gamma < 1$. Further, it is noted that $C_{fx}(0)$ decreases for the increasing values of *M* and $S < 0$ whereas increases for the increasing values of $S > 0$ when $\gamma > 1$. It is interesting to note that $-q'(0)$, $-f'(0)$ and $C_{fx}(0)$ show quite opposite behavior for the increasing values of *M* in both cases of $\gamma < 1$ and $\gamma > 1$.

Table 1: Comparison of the reduced Nusselt number $-q'(0)$ and the reduced Sherwood number $-f'(0)$ when $M = \gamma = S = \delta = R = 0$ and Pr = *Le* = 10.

		Khan and Pop [28]		Present Results	
Nb	*Nt*	$-q'(0)$	$-f'(0)$	$-q'(0)$	$-f'(0)$
0.1	0.1	0.9524	2.1294	0.9524	2.1294
0.2	0.2	0.3654	2.5152	0.3654	2.5152
0.3	0.3	0.1355	2.6088	0.1355	2.6088
0.4	0.4	0.0495	2.6038	0.0495	2.6038
0.5	0.5	0.0179	2.5731	0.0179	2.5731

Figs. 2 and 3 show the effects of *M* and *S* on $f'(h)$ when $\gamma < 1$ and $\gamma > 1$. From these Figs. it is noticed that $f'(h)$ decreases for the increasing values of *M* and *S* when $\gamma < 1$ while an opposite effect is noted for the case when $\gamma > 1$. This behavior is due to the fact that increasing values of *M* increases the resistive forces on the sheet which reduces the fluid velocity and hence the motion of the fluid is slow down. It is further noticed that increasing values of *M* and *S* give no change in $f'(h)$ which shows that the momentum boundary layer is not influenced in the case when external stream velocity becomes equal to the stretching velocity. This causes for a frictionless flow called the Hiemenz flow [27]. It is also observed from these Figs. that $f'(h)$ increases for increasing values of γ.

Table 2: Variations of the reduced Nusselt number $-q'(0)$, the reduced Sherwood number $-f'(0)$ and skin-friction coefficient $C_{fx}(0)$.

Nb	*Nt*	Pr	*Le*	*M*	*R*	γ	*S*	δ	$-q'(0)$	$-f'(0)$	$C_{fx}(0)$
0.1	0.1	1.0	10	0.1	1.0	0.1	0.1	0.1	0.4918	4.4601	1.0568
0.5	0.1	1.0	10	0.1	1.0	0.1	0.1	0.1	0.3376	4.4872	1.0568
0.1	0.5	1.0	10	0.1	1.0	0.1	0.1	0.1	0.3978	4.5693	1.0568
0.1	0.1	10	10	0.1	1.0	0.1	0.1	0.1	0.9272	4.6867	1.0568
0.1	0.1	1.0	20	0.1	1.0	0.1	0.1	0.1	0.4902	6.7375	1.0568
0.1	0.1	1.0	10	2.5	1.0	0.1	0.1	0.1	0.3909	4.4195	1.7660
0.1	0.1	1.0	10	2.5	1.0	1.1	0.1	0.1	0.7250	4.5434	-0.2328
0.1	0.1	1.0	10	0.1	3.0	0.1	0.1	0.1	0.4905	6.4806	1.0568
0.1	0.1	1.0	10	0.1	1.0	0.6	0.1	0.1	0.6196	4.4890	0.5921
0.1	0.1	1.0	10	0.1	1.0	1.1	0.1	0.1	0.7226	4.5403	-0.1728
0.1	0.1	1.0	10	0.1	1.0	1.6	0.1	0.1	0.8112	4.6047	1.1656
0.1	0.1	1.0	10	0.1	1.0	0.1	0.5	0.1	0.7554	7.1516	1.2638
0.1	0.1	1.0	10	0.1	1.0	0.1	-0.5	0.1	0.1672	1.8471	0.8050
0.1	0.1	1.0	10	0.1	1.0	1.1	0.5	0.1	0.9695	7.1997	-0.1963
0.1	0.1	1.0	10	0.1	1.0	1.1	-0.5	0.1	0.4069	1.9175	0.1417
0.1	0.1	1.0	10	0.1	1.0	0.1	0.1	0.3	0.2539	4.5312	1.0568
0.1	0.1	1.0	10	0.1	1.0	0.1	0.1	-0.5	0.7765	4.3508	1.0568

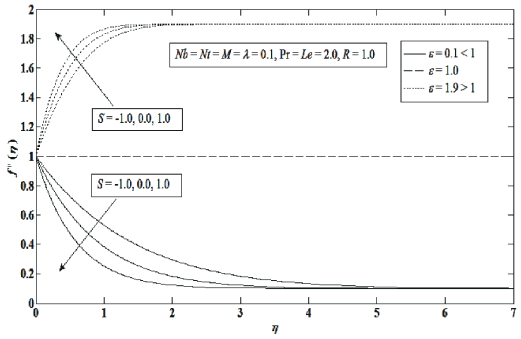

Fig. 2: Variations of velocity profiles along 0 for various values of *M*.

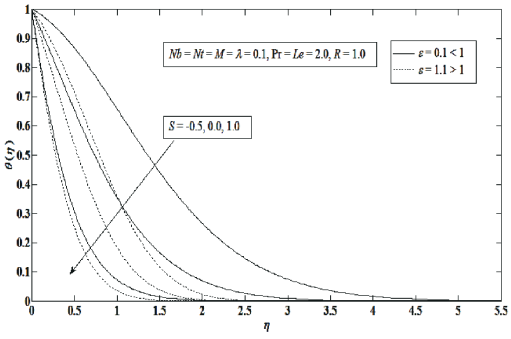

Fig. 6: Variations of temperature profiles along 0 for various values of *S*.

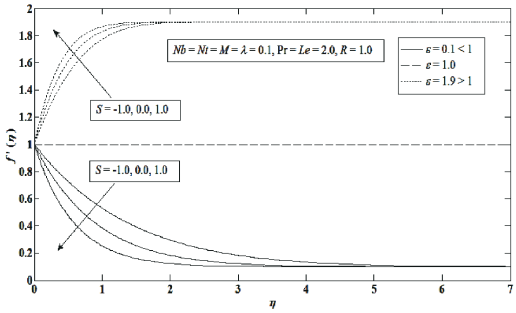

Fig. 3: Variations of velocity profiles along 0 for various values of *S*.

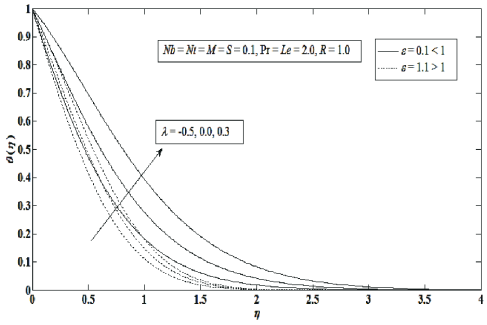

Fig. 7: Variations of temperature profiles along 0 for various values of 8.

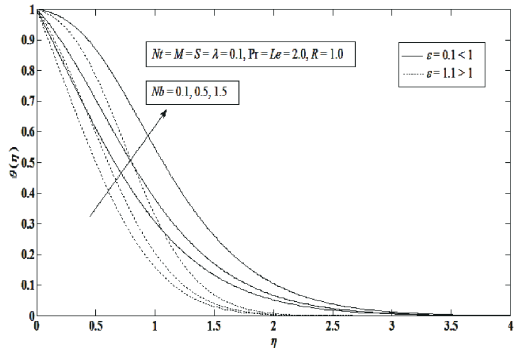

Fig. 4: Variations of temperature profiles along 0 for various values of *Nb*.

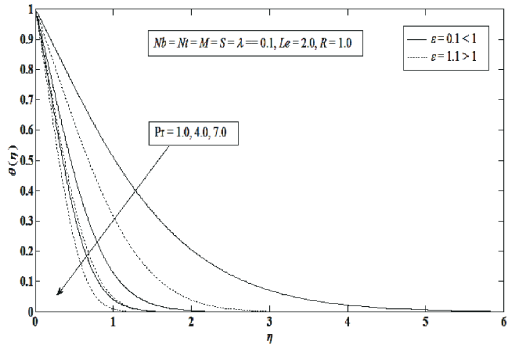

Fig. 8: Variations of temperature profiles along 0 for various values of Pr.

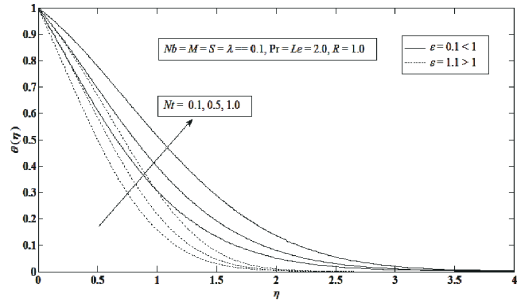

Fig. 5: Variations of temperature profiles along 0 for various values of *Nt*.

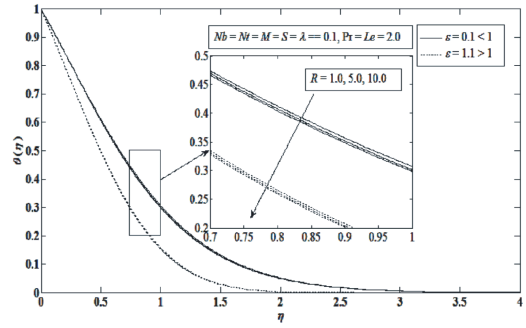

Fig. 9: Variations of temperature profiles along 0 for various values of *R*.

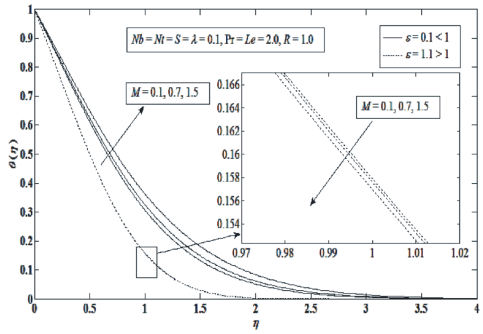

Fig. 10: Variations of temperature profiles along η for various values of *M*.

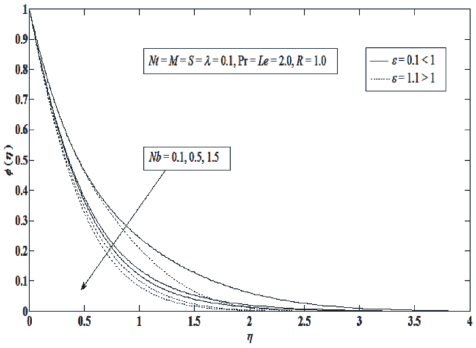

Fig. 11: Variations of concentration profiles along η for various values of *Nb*.

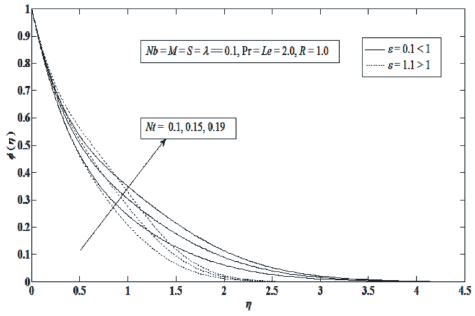

Fig. 12: Variations of concentration profiles along η for various values of *Nt*.

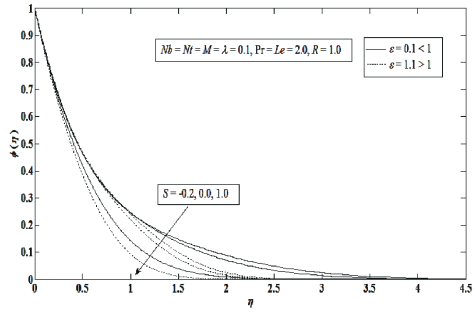

Fig. 13: Variations of concentration profiles along η for various values of *S*.

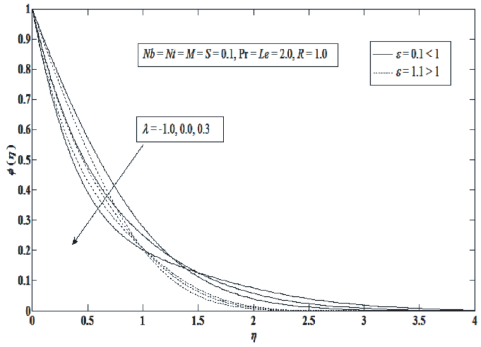

Fig. 14: Variations of concentration profiles along η for various values of δ.

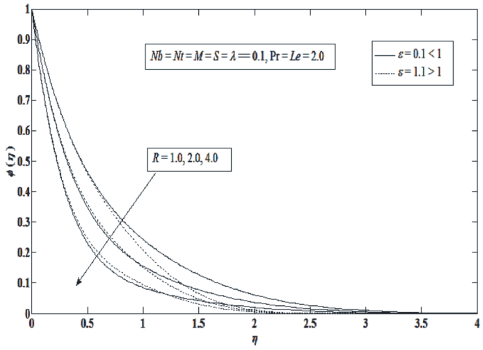

Fig. 15: Variations of concentration profiles along η for various values of *R*.

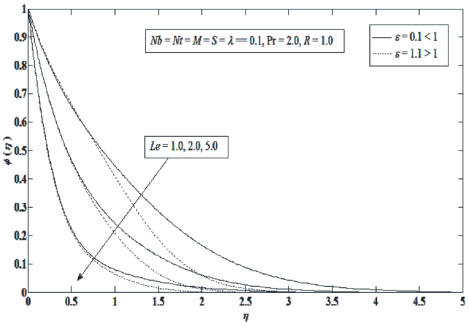

Fig. 16: Variations of concentration profiles along η for various values of *Le*.

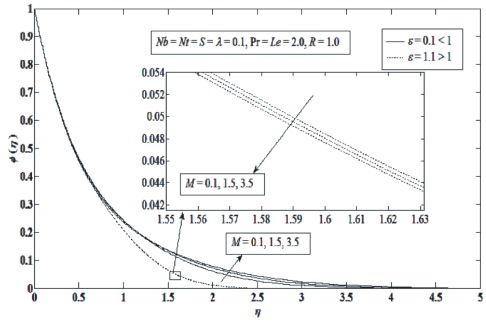

Fig. 17: Variations of concentration profiles along η for various values of *M*.

Figs. 4 to 9 illustrate that $q(h)$ increases for the increasing values of *Nb*, *Nt* and δ whereas decreases for the increasing values of Pr, *S* and *R*. Such behaviour of Pr depends upon the formation of nanofluid which is a combination of the base fluid (water, oil and ethylene glycol) and nanoparticles (Cu, Aluminium, Titanium) influences on. The increasing values of Pr increase the viscosity of the base fluid which results for a decrease in the thermal boundary layer thickness and consequently heat transfer decreases for the larger values of Pr. This is due to the reason that highly viscous nanofluid (with large values of Pr) results for low thermal conductivities affecting the conduction phenomenon to shorten the thermal boundary layer thickness. Also, the suspended nanoparticle motions are more affected in the highly viscous nanofluid due to less colloidal forces among each other. Fig. 10 shows that $q(h)$ increases for the increasing values of *M* when $\gamma < 1$ whereas decreases when $\gamma > 1$. It is worth mentioning here that, the large values of *M* and *R* show minimal changes in $q(h)$ when $\gamma > 1$.

Figs. 11 to 17 are plotted for $f(h)$ to analyze the effects of *Nb*, *Nt*, *M*, *S*, *R*, δ and *Le* in both cases of $\gamma < 1$ and $\gamma > 1$. It is observed from Figs. 11 to 16 that $f(h)$ decreases for the increasing values of *Nb*, *S*, δ, *R* and *Le* but increases for the increasing values of *Nt*. Fig. 17 illustrate that $f(h)$ increases for the increasing values of *M* when $\gamma < 1$ while decreases for the case when $\gamma > 1$. Also, the above discussed Figs. show that concentration boundary layer thickness is greater for the case when $\gamma < 1$ as compare to the case when $\gamma > 1$. Also, the large values of *M* shows a minimal change in $f(h)$ when $\gamma > 1$. Since all the above discussed profiles descend smoothly in the free stream satisfying the boundary conditions that ensure the accuracy of the obtained numerical results.

CONCLUSION

In the present study, chemical reaction and heat generation/absorption effects on MHD stagnation-point flow of a nanofluid over a porous sheet were investigated. The presented nanofluid model incorporates the effects of Brownian motion parameter *Nb*, thermophoresis parameter *Nt*, Prandtl number Pr, Lewis number *Le*, Hartmann number *M*, velocity ratio parameter γ, heat source or sink parameter δ, suction or injection parameter *S* and chemical reaction parameter *R*. The governing nonlinear partial differential equations were transformed into nonlinear ordinary differential equations by using similarity transformation and then solved numerically using an implicit finite difference scheme known as Keller-box method. The numerical results depending upon incorporated flow parameters were presented in tables and Figs. For the accuracy purpose, the present results were compared with already published results of Khan and Pop [28] and found in a good agreement. The main conclusions are as below:

- The magnitude of skin-friction coefficient C_{fx} (0) is zero for $\gamma = 1$. However, for increasing values of *M* and *S*, velocity profiles were observed in inverted manner for both cases of $\gamma < 1$ and $\gamma > 1$ but these profiles were found increased for the increasing values of γ. The results showed that C_{fx} (0) decreases for the increasing values of *M* and $S < 0$ whereas increases for the increasing values of $S > 0$.
- Further, $-f'(0)$ increases for the increasing values of $S > 0$, $\delta < 0$ and decreases for increasing values of *R*, $S < 0$ and $\delta > 0$. Whereas, $-f'(0)$ decreases for the increasing values of $S < 0$, $\delta < 0$ and increases for increasing values of *R*, $S > 0$ and $\delta > 0$.
- It is noted that increasing values of *M* showed quite opposite behavior in C_{fx}(0), $-q'(0)$ and $-f'(0)$ for both cases of $\gamma < 1$ and $\gamma > 1$.
- Also, increase in $-q'(0)$ and $-f'(0)$ against *M*, δ and *R* is less in the case of $\gamma < 1$ compared to $\gamma > 1$.
- Momentum, thermal and concentration boundary layers are found shortened and approaching to zero more rapidly in the case of $\gamma > 1$ compared to $\gamma < 1$.

ACKNOWLEDGEMENTS

The authors would like to acknowledge the financial support received from MOE, Research Management Centre Universiti Teknologi Malaysia (4F109) and Universiti Malaysia Pahang (RDU110108).

REFERENCES

1. Das, S.K., S.U.S. Choi, W. Yu and T. Pradeep, 2007. Nanofluids: Science and Technology. U.S.A: Wiley.
2. Anwar, M.I., I. Khan, A. Hussanan, M.Z. Salleh and S. Sharidan, 2013. Stagnation-point flow of a nanofluid over a nonlinear stretching sheet. World App. Sci. J., 23: 998-1006.

3. Chandrasekar, M. and S. Suresh, 2009. A review of the mechanisms of heat transport in nanofluids. Heat Transf. Engg., 30: 1136-1150.
4. Choi, S.U.S., Z.G. Zhang, W. Yu, F.E. Lockwood and E.A. Grulke, 2001. Anomalously thermal conductivity enhancement in nanotube suspensions. Appl. Phys. Lett., 79: 2252-2254.
5. Putra, N., W. Roetzel and S.K. Das, 2003. Natural convection of nanofluids, Heat Mass Transf., 39: 775-784.
6. Kuznetsov, A.V. and D. A. Nield, 2010. Natural convective boundary-layer flow of a nanofluid past a vertical plate. Int. J. Therm. Sci., 49: 243-247.
7. Rana, P. and R. Bhargava, 2012. Flow and heat transfer of a nanofluid over a nonlinearly stretching sheet: A numerical study. Commun. Nonlinear Sci. Numer. Simul., 17: 212-226.
8. Jafar, K., A. Ishak and R. Nazar, 2012. MHD stagnation-point flow over a nonlinearly stretching or shrinking sheet. J. Aerospace Engg. doi:10.1061/ (ASCE) AS. 1943-5525. 0000186.
9. Nadeem, S. and C. Lee, 2012. Boundary layer flow of nanofluid over an exponentially stretching surface, Nano. Research Lett., 94: 1-8.
10. Anwar, M.I., I. Khan, S. Sharidan and M.Z. Salleh, 2012. Conjugate effects of heat and mass transfer of nanofluids over a nonlinear stretching sheet, Int. J. Phys. Sci., 7: 4081-4092.
11. Chen, C.H., 2008. Effects of magnetic field and suction or injection on convection heat transfer of non-Newtonian power law fluids past a power law stretched sheet with surface heat flux. Int. J. Therm. Sci., 47: 954-961.
12. Mustafa, M., T. Hayat, I. Pop, S. Asghar and S. Obaidat, 2011. Stagnation-point flow of a nanofluid towards a stretching sheet. Int. J. Heat Mass Transf., 54: 5588-5594.
13. Chamkha, A.J. and A.M. Alymhd, 2011. Free convection flow of a nanofluid past a vertical plate in the presence of heat generation or absorption effects, Chem. Eng. Comm., 198: 425-441.
14. Muthucumaraswamy, R., 2012. Chemical reaction effects on vertical oscillating plate with variable temperature, Chem. Ind. Chem. Eng. Quart., 16: 167-173.
15. Muthucumaraswamy, R. and K. Manivannan, 2011. First order chemical reaction on isothermal vertical oscillating plate with variable mass diffusion, Int. J. Pure Appl. Sci. Technol., 3: 19-26.
16. Chamkha, A.J. and C. Issa, 2000. Effects of heat generation or absorption and thermophoresis on hydromagnetic flow with heat and mass transfer over a flat surface. Int. J. Numer. Method. Heat. Fluid Flow., 10: 432- 449.
17. Makinde, O.D. and A. Aziz, 2011. Boundary layer flow of a nanofluid past a stretching sheet with a convective boundary condition, Int. J. Therm. Sci., 50: 1326-1332.
18. Alsaedi, A., M. Awais and T. Hayat, 2012. Effects of heat generation/absorption on stagnation point flow of nanofluid over a surface with convective boundary conditions, Commun. Nonlinear Sci. Numer. Simul., 17: 4210 - 4223.
19. Ferdows, M., M.S. Khan, M.M. Alam and S. Sun, 2012. MHD mixed convective boundary layer flow of a Nanofluid through a porous medium due to an exponentially stretching sheet, Math. Probl. Eng., pp: 1-21, doi:10.1155/2012/408528.
20. Uddin, M.J., W.A. Khan and A.I.M. Ismail, 2012. Scaling group transformation for MHD boundary layer slip flow of a nanofluid over a convectively heated stretching sheet with heat generation, Math. Probl. Eng., 2012, Article ID 934964, doi:10.1155/2012/934964.
21. Kandasamy, R., I. Muhaimin and H.B. Saim, 2010. Lie group analysis for the effect of temperature-dependent fluid viscosity with thermophoresis and chemical reaction on MHD free convective heat and mass transfer over a porous stretching surface in the presence of heat source/sink, Commun. Nonlinear Sci. Numer. Simul., 15: 2109-2123.
22. Ouaf, M.E.M., 2005. Exact solution of thermal radiation on MHD flow over a stretching porous sheet. Appl. Math. Comput., 170: 1117-1125.
23. Hamad, M.A.A. and M. Ferdows, 2012. Similarity solution of boundary layer stagnation-point flow towards a heated porous stretching sheet saturated with a nanofluid with heat absorption or generation and suction or blowing: A Lie Group Analysis. Commun. Nonlin. Sci. Numer. Simul., 17: 132-140.
24. Ding, Y., H. Chen, L. Wang, C.Y. Yang, Y. He, W. Yang, W.P. Lee, L. Zhang and R. Huo, 2007. Heat transfer intensification using nanofluids. Kona., 25: 23-38.
25. Kumar, H., 2013. Heat and mass transfer over an isothermal inclined plate at constant concentration gradient and with heat source. World App. Sci. J., 24: 364-369.

26. Cebeci, T. and P. Bradshaw, 1988. Physical and computational aspects of convective heat transfer. Springer-Verlag, New York.
27. Yacob, N.A. and A. Ishak, 2012. Stagnation-point Flow towards a Stretching or Shrinking sheet in a Micropolar Fluid with a Convective Surface Boundary Condition. Canad. J. Chem. Engg., 90: 621-626.
28. Khan, W.A. and I. Pop, 2012. Boundary layer flow of a nanofluid past a stretching sheet. Int. J. Heat Mass Transf., 53: 2477-2483.